Engineering Notes

ENGINEERING NOTES are short manuscripts describing new developments or important results of a preliminary nature. These Notes cannot exceed 6 manuscript pages and 3 figures; a page of text may be substituted for a figure and vice versa. After informal review by the editors, they may be published within a few months of the date of receipt. Style requirements are the same as for regular contributions (see inside back cover).

Leading-Edge Force Features of the Aerodynamic Finite Element Method

CHUAN-TAU LAN* AND JAN ROSKAM†
University of Kansas, Lawrence, Kansas

Introduction

THE aerodynamic finite-element method has been shown to be a reliable tool in analyzing the aerodynamic characteristics of complete airplane configurations.[1,2] However, these methods do not account for the leading-edge thrust at subsonic speeds and at supersonic speeds with subsonic leading edges. At subsonic speeds, there exist several methods of evaluating the leading-edge thrust distribution in the literature. Garner, Hewitt and Labrujere compared the computing efficiency of the methods of NPL, BAC and NLR.[3] Wagner's method[4] and Lamar's method[5] also included the leading-edge thrust computation. The current vortex lattice method seems in most cases to predict an induced drag parameter which is less than the minimum value, or $1/(\pi A)$, so that a scaling factor is required to evaluate correctly the suction distribution.[6] All these methods are applicable only to planar wings, except the vortex lattice method which may be applied to cases with fuselage of circular cylindrical cross section and with nonplanar tail location. At supersonic speeds, no methods seem to be available for arbitrary planform shapes including nonplanar tail and fuselage effects.

In this Note, a practical method of computing the leading-edge thrust distribution by finite element method is formulated. When incorporated into a wing-body aerodynamic computer program, the present method is capable of predicting at subsonic and supersonic speeds the leading-edge thrust distribution (and therefore, the lateral-directional stability derivatives due to roll) and the nonlinear aerodynamic characteristics of low aspect-ratio wings with leading-edge separation through the application of suction analogy.

Method

The leading-edge suction forces per unit length of the leading edge are given by the following expressions[7]

$$X = -(\pi/8)q_\infty(1 - M_\infty{}^2 \cos^2\Lambda_{\text{L.E.}})^{1/2} \times (\Delta C_p)^2(x - x_{\text{L.E.}})\,|\,x \to x_{\text{L.E.}} \qquad (1)$$

$$Y = X \tan\Lambda_{\text{L.E.}} \qquad (2)$$

In Eqs. (1) and (2), q_∞ is the freestream dynamic pressure, M_∞ the freestream Mach number, $\Lambda_{\text{L.E.}}$ the local leading-edge sweep angle and ΔC_p the difference in the pressure coefficients. The x axis is positive downstream and the y axis is positive to the right. The ΔC_p values near the leading edge are obtained by extrapolation from the discrete ΔC_p values computed with the finite-element method and are given by the following expression

$$\Delta C_p = (1 - \xi)^{1/2}\xi^{-1/2}f(\xi) \qquad (3)$$

where ξ is the nondimensional x coordinate measured in local chord length from the local leading edge and $f(\xi) = a_o + a_1\xi + a_2\xi^2 + \ldots$, where a_o, a_1, etc. are obtained by interpolation of the computed discrete ΔC_p values. The number of unknowns retained in $f(\xi)$ equals the number of chordwise panels used. The sectional leading-edge thrust coefficient is therefore given by

$$c_t = X \,.\, \Delta l/(q_\infty c \Delta y) = -(\pi/8)(\Delta l/\Delta y)(1 - M_\infty{}^2 \cos^2\Lambda_{\text{L.E.}})^{1/2}(\Delta C_p)^2\xi\,|_{\xi\to 0} \qquad (4)$$

To evaluate the static aeroelastic effect on the leading-edge thrust distribution, it is known that the pressure distribution after aeroelastic distortion is given by[7]

$$(\Delta C_p) = (\Delta s)^{-1}[(1) - q_\infty(A)(C_\theta)]^{-1}(A)\{\alpha - (C_\theta)(m)g\} \qquad (5)$$

where Δs is the aerodynamic panel area, (1) the identity matrix, (A) the aerodynamic influence coefficient matrix, (C_θ) the structural influence coefficient matrix, m the aerodynamic panel mass and g the gravitational acceleration. To compute the induced drag distribution, the new inclination of each panel to the freestream is needed. This new inclination is the sum of the original angle of attack and the elastic distortion angle θ_E given by

$$(\theta_E) = [(1) - q_\infty(C_\theta)(A)]^{-1}(C_\theta)[q_\infty(A)(\alpha) - (m)g] \qquad (6)$$

It has been found that the total lift and moment coefficients predicted by the finite-element method are not too sensitive to the chordwise paneling scheme. However, an accurate pressure distribution can be obtained only if smaller panels are used near the leading edge. Define l_i as the distance from the trailing boundary of the ith panel to the wing leading edge referred to the local chord length. Then $l_o = 0$ is the wing leading edge. Woodward[1] has successfully used the scheme $(l_i) = (0, 5, 15, 25, 35, 45, 55, 65, 75, 85, 100)$ for 10 chordwise panels. However, it was found in the present study that the induced drag parameter $C_{Di}/C_L{}^2$ cannot be correctly predicted by the Woodward's scheme, because the accuracy of $C_{Di}/C_L{}^2$ by that scheme depends on the aspect ratio, the sweep angle and the Mach number. It was also found not necessary to always use 100 panels for the half wing to predict accurately the lift coefficient. To save computing cost yet retain accuracy, 80 panels over the half wing were used in the present study, with 10 approximately equal spanwise strips and 8 chordwise rows. With 8 chordwise rows, the average chordwise panel size is 12.5 (or 100/8)% of the local chord. Since it is essential to use smaller panels near the leading edge, it was decided to increase the panel sizes gradually toward the trailing edge, as given by the following scheme

$$l_i = 0, l_2, 12, 21, 33, 48, 63, 81, 100, \qquad i = 0, 1, \ldots, 9 \qquad (7)$$

l_2 was assumed to depend only on aspect ratio, sweep angle and Mach number. If l_2 is 5% on the average, then the panel sizes in percentage of the local chord given by Eq. (7) would be 5, 7, 9, 12, 15, 15, 18 and 19. Correct value for l_2 is obtained by correlation, as described below. Three planforms with known $C_{Di}/C_L{}^2$ each were chosen for correlation in subsonic

Received May 18, 1972; revision received July 25, 1972. This Note is based partially on the research sponsored by NASA under Grant NGR 17-002-071.
Index category: Airplane and Component Aerodynamics.

* Assistant Professor of Aerospace Engineering. Member AIAA.
† Professor of Aerospace Engineering. Associate Fellow AIAA.

Table 1 Comparison of computed induced drag parameters by various methods

Planforms	A	M_∞	Methods	C_{Di}/C_L^2	References
Variable-sweep wing	4.303	0.23	Wagner Present	0.075 0.07918	4
Warren 12	$2(2)^{1/2}$	0.0	NLR wake integral Present	0.11344 0.12079	3
Cropped double delta	3.436	0.0	Wake integral Present	0.09270 0.09298	5 (p. 58)
Highly swept and tapered	1.697	0.28	Wake integral Present	0.188 0.18992	5 (p. 71)
Constant chord swept-back	2.0	$(2)^{1/2}$	Exact Present	0.24 0.24	8
Constant chord swept-back	2.24	1.2289	Exact Present	0.20714 0.2080	8
Double delta	3.2023	2.0	Exact Present	0.4403 0.43979	9
Double delta	3.0077	$(2)^{1/2}$	Exact Present	0.229 0.22471	9

and supersonic flows. For the subsonic case, these known results are from wake integrals by other theoretical methods. For the supersonic case, exact linear results for simple planforms were used (two aspect ratios and two sweep angles). The Mach number effect was included through the Prandtl-Glauert Transformation. l_2 was determined so that the computed C_{Di}/C_L^2 for each of the three planforms agreed with the other theoretical results as closely as possible. From these correlations, formulas for l_2 were found by linear interpolation or extrapolation for the effects of aspect ratios and sweep angles. For wings in subsonic flow, it can be shown that

$$l_2 = 4.796 + 0.0816(\beta A - 2) - 0.00791 \tan^{-1}[(1/\beta) \tan\Lambda_{L.E.}] \tag{8}$$

$$\beta = (1 - M_\infty{}^2)^{1/2}$$

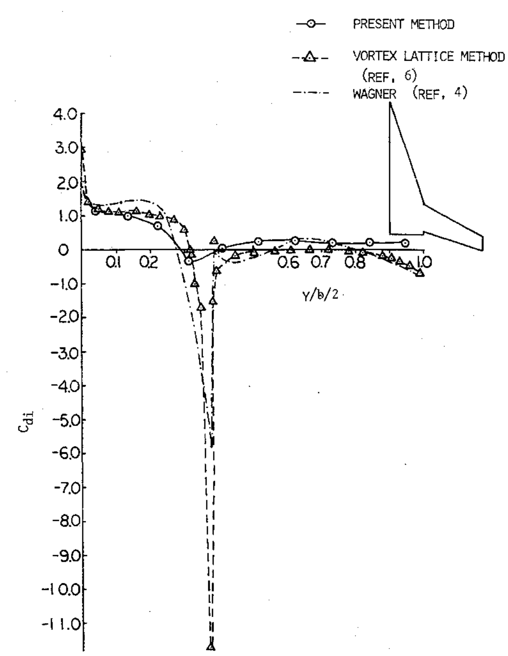

Fig. 1 Comparison of spanwise induced drag distribution for a variable sweep wing of $A = 4.303$, $\alpha = 1$ rad, $M_\infty = 0.23$.

For wings in supersonic flows, it can be shown that

$$l_2 = 4.83 + 0.10875(\beta A - 3.3333) + 0.135165[\tan^{-1}[(1/\beta) \tan \Lambda_{L.E.}] - 68.198] \tag{9}$$

$$\beta = (M_\infty{}^2 - 1)^{1/2}$$

In Eqs. (8) and (9), the arctangent function is to be expressed in degrees. Note that for variable sweep wings, $\Lambda_{L.E.}$ must be the leading-edge sweep angle of that portion which has larger dimensions in the spanwise direction. In case two portions have the same dimension in the spanwise direction, the outer leading-edge sweep angle is to be used. The numbers given in Eq. (7) can be changed in any reasonable way and the computed values correlated with known results to obtain a different set of expressions for l_2. Once this is done, the same scheme can be applied successfully to other planforms, as indicated by results shown below.

Verification and Applications

Extensive comparison with other theoretical results in predicting C_{Di}/C_L^2 has been made.[7] Some of these comparisons are shown in Table 1. It is seen that the present method always gives reasonable results. The spanwise induced drag distribution for three planforms in Ref. 6 at subsonic speeds has also been compared. They all show good agreement.[7] For the variable sweep wing, see Fig. 1. In this case, the strong variation in the induced drag distribution near the leading-edge crank has not been predicted by the present method with 10 spanwise strips due to insufficient number of panels near the crank. The induced drag distribution for a delta wing is compared in Fig. 2. Another way of showing the correct leading-edge thrust distribution is to compare the predicted lateral-directional stability drivatives due to roll. When referred to body axes, the lateral force and yawing moment due to steady roll arise entirely from suction forces along the wing edges. The delta wing of $A = 10/3$ at

Table 2 Comparison of predicted C_{np}, C_{pl} and C_{pY} for a delta wing at $M_\infty = {}^{1/2}(2)$

Derivatives	Exact[10]	Present method
$C_{Yp}/$	0.7066	0.6959
C_{np}/α	−0.5388	−0.5233
C_{lp}	−0.2911	−0.2816

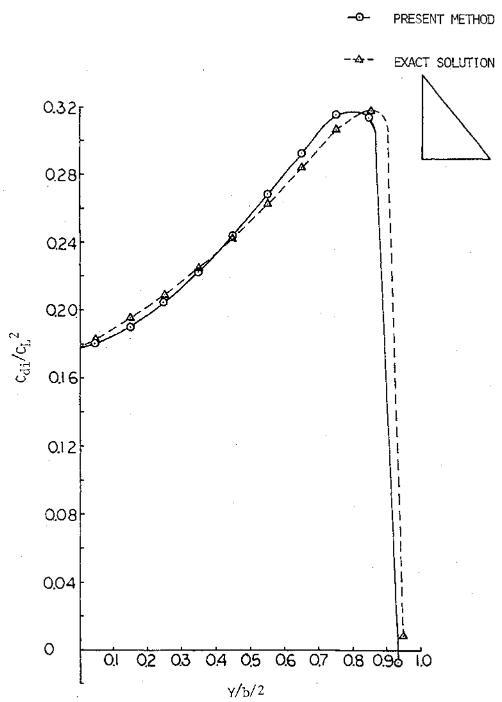

Fig. 2 Comparison of spanwise induced drag distribution for a delta wing of $A = 3.333$, $\alpha = 0.1$ rad, $M_\infty = (2)^{1/2}$.

$M_\infty = (2)^{1/2}$ was chosen for comparison, as the exact solution is available. Results are presented in Table 2, together with C_{l_p} for completeness. It is seen that the present results show good agreement with exact values.

Another verification and application of the present method is the prediction of nonlinear aerodynamic characteristics with leading-edge separation through the application of suction analogy.[7] The results for a delta wing of $A = 1.147$ and an arrow wing of $A = 1.463$ both at $M_\infty = 0.2$ show excellent agreement with Polhamus' Method.[11] The results for a delta wing of $A = 1.0$ at $M_\infty = 1.97$ are compared in Fig. 3.

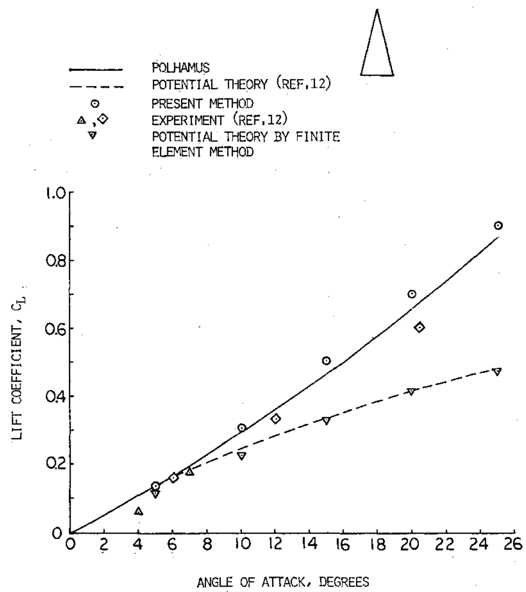

Fig. 3 Comparison of theoretical and experimental lift characteristics for a delta wing of $A = 1.0$ at $M_\infty = 1.97$.

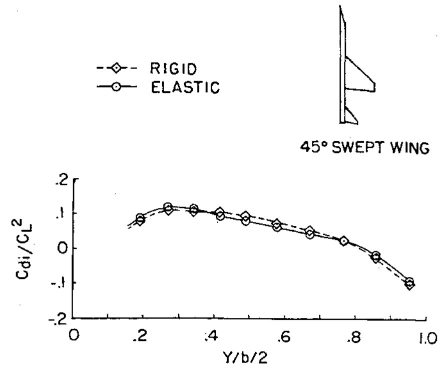

Fig. 4 Rigid and elastic spanwise induced drag distribution on the wing surface for a wing-body-tail combination at $M_\infty = 0.8$ at sea level.

After establishing the validity of the present formulation, it is then applied to the prediction of the static aeroelastic effects on the induced drag. The results for a wing-body tail combination with 45°-sweep wing at sea level are shown in Table 3. The structural influence coefficient matrix was obtained by beam theory, assuming that both wing and tail are of the two-spar construction. The airplane mass distribution was assumed to have the typical values used in Ref. 13. The fuselage is assumed to be a flat plate which does not contribute to leading-edge thrust. The tail surface was divided into 30 panels with 6 rows chordwise. The paneling scheme was obtained by a similar type of correlation. It is seen that due to the aeroelastic unloading, both $C_{L\alpha}$ and C_{Di} are reduced by structural flexibility. On the other hand, the induced drag parameters C_{Di}/C_L^2 are increased. The induced drag distribution for $M_\infty = 0.8$ is illustrated in Fig. 4.

References

[1] Woodward, F. A., "Analysis and Design of Wing-Body Combinations at Subsonic and Supersonic Speeds," *Journal of Aircraft*, Vol. 5, No. 6, Nov.-Dec. 1968, pp. 528–534.

[2] Bradley, R. G. and Miller, B. D., "Application of Finite-Element Theory to Airplane Configurations," *Journal of Aircraft*, Vol. 8, No. 6, June 1971, pp. 400–405.

[3] Garner, H. C., Hewitt, B. L., and Labrujere, T. E., "Comparison of Three Methods for the Evaluation of Subsonic Lifting-Surface Theory," R&M 3597, June 1968, Aeronautical Research Council, Great Britain.

[4] Wagner, S., "On the Singularity Method of Subsonic Lifting-Surface Theory," *Journal of Aircraft*, Vol. 6, No. 6, Nov.-Dec. 1969, pp. 549–558.

[5] Lamar, J. E., "A Modified Multhopp Approach for Predicting Lifting Pressures and Camber Shape for Composite Planforms in Subsonic Flow," TN D-4427, July 1968, NASA.

[6] Karman, T. P., Giesing, J. P., and Rodden, W. P., "Spanwise Distribution of Induced Drag in Subsonic Flow by the Vortex Lattice Method," *Journal of Aircraft*, Vol. 7, No. 6, Nov.-Dec. 1970, pp. 574–576.

[7] Lan, C., Mehrotra, S., and Roskam, J., "Leading-Edge Force Features of the Aerodynamic Finite Element Method," CRINC-FRL Rept. 72-007, April 1972, Center for Research Inc., The Univ. of Kansas, Lawrence, Kansas.

[8] Cohen, D., "Formulas for the Supersonic Loading, Lift and Drag of Flat Swept-Back Wings with Leading Edges Behind the Mach Lines," TN 1860, 1949, NACA.

Table 3 Comparison of rigid and elastic aerodynamic properties for a wing-body-tail combination at sea level

	$M_\infty = 0.8$			$M_\infty = 1.5$		
	$C_{L\alpha}$, rad^{-1}	C_{Di}	C_{Di}/C_L^2	$C_{L\alpha}$, rad^{-1}	C_{Di}	C_{Di}/C_L^2
Rigid	3.7998	1.5922	0.11027	3.8946	3.8946	0.25677
Elastic	3.2906	1.3923	0.12859	2.3306	1.8991	0.34963

[9] Cohen, D. and Friedman, M. D., "Theoretical Investigation of the Supersonic Lift and Drag of Thin, Swept-Back Wings with Increased Sweep Near the Root," TN 2959, 1953, NACA.

[10] Ribner, H. S. and Malvestuto, F. S., Jr., "Stability Derivatives of Triangular Wings at Supersonic Speeds," Rept. 908, 1948, NACA.

[11] Davenport, E. E. and Huffman, J. K., "Experimental and Analytical Investigation of Subsonic Longitudinal and Lateral Aerodynamic Characteristics of Slender Sharp-Edge 74° Swept Wings," TN D-6344, 1971, NASA.

[12] Polhamus, E. C., "Predictions of Vortex-Lift Characteristics Based on a Leading-Edge Suction Analogy," *Journal of Aircraft*, Vol. 8, No. 4, April 1971, pp. 193–199.

[13] "A Parametric Study of Planform and Aeroelastic Effects on Aerodynamic Center, α- and q-Stability Derivatives," CRINC-FRL 72-002, Feb. 1972, The Flight Research Lab., Univ. of Kansas, Lawrence, Kansas, NASA Contractor Report, to be published.

Load-Time Dependent Relaxation of Residual Stresses

DARRELL SIMPKINS,* ROBERT L. NEULIEB,* AND DENNIS J. GOLDEN†
Air Force Flight Dynamics Laboratory, Wright-Patterson Air Force Base, Ohio

Introduction

A DIFFICULTY in the structural design of aircraft with respect to preventing fatigue failures is the application of data obtained from tests of a few days duration for the prediction of aircraft life of several years. One commonly observed phenomenon in specimen test is life lengthening due to compressive residual stresses which occur as a result of plastic tensile deformation at a stress concentration.[1–4] In a recent test of an aluminum alloy, a load-time relaxation of residual stresses which shortened the life of a specimen has been experimentally observed. These results are in contrast to those obtained by Smith[5] and Gassner (reported by Schijve[6]) where no significant decrease in life was observed. In these latter tests only time dependent relaxation was studied, since the specimens were unloaded during hold periods.

The current cyclic tests were conducted to determine the influence on residual stress benefits due to applying compressive loads to specimens, holding these loads for specified time periods, and then cycling to failure. These tests were conducted as a part of a larger program investigating, among other effects, appropriate high end truncation levels for flight simulation laboratory fatigue tests. Spectra selected for this program were representative of transport lower wing surface location loadings.

Test Procedures and Results

The specimens tested were center hole specimens as shown in Fig. 1. The theoretical stress concentration factor was 2.54 based on net section stresses. The material was aluminum 7075-T651 bare.

Received July 25, 1972.
Index categories: Properties of Materials; Aircraft Structural Design (Including Loads).

† Captain U. S. Air Force; Aerospace Engineer, Design Methodology Group, Design Criteria Branch.
* Aerospace Engineer, Design Methodology Group, Design Criteria Branch.

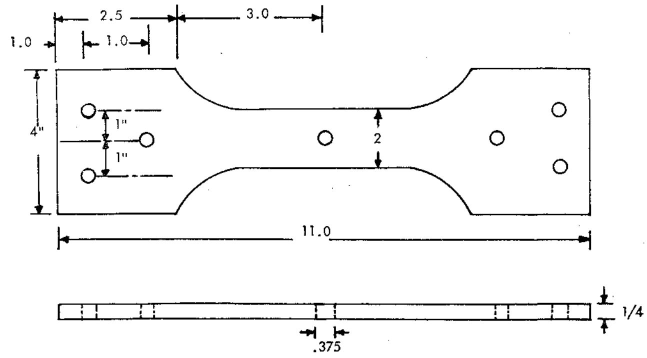

Fig. 1 Specimen geometry.

The test load sequences were as shown in Fig. 2. Test sequences 1 and 2 were run to establish baseline data for comparison with results for test sequences 3 and 4. The constant amplitude loading varied from 5–25 KSI net section stress in all four sequences. The single preload was 45 KSI net section stress in all four sequences while the compressive load in sequence 2 and the compressive load held for a specified time in sequences 3 and 4 was −7.5 KSI net section stress. The single hold period in sequence 3 and the two hold periods in sequence 4 were of 24 hours duration each. Between the two hold periods in sequence 4, 3000 constant amplitude cycles were applied. The sequences were applied to specimens in laboratory air except during the hold periods when the temperature was controlled at 85°F. Constant amplitude loads were applied at a rate of 5 Hz.

The results of these tests are given in Table 1.

Discussion

The results presented in Table 1 indicate that all benefits due to compressive residual stresses observed in aluminum specimen tests of a few days duration may not be observed in actual aircraft lower wing surface structures which sustain

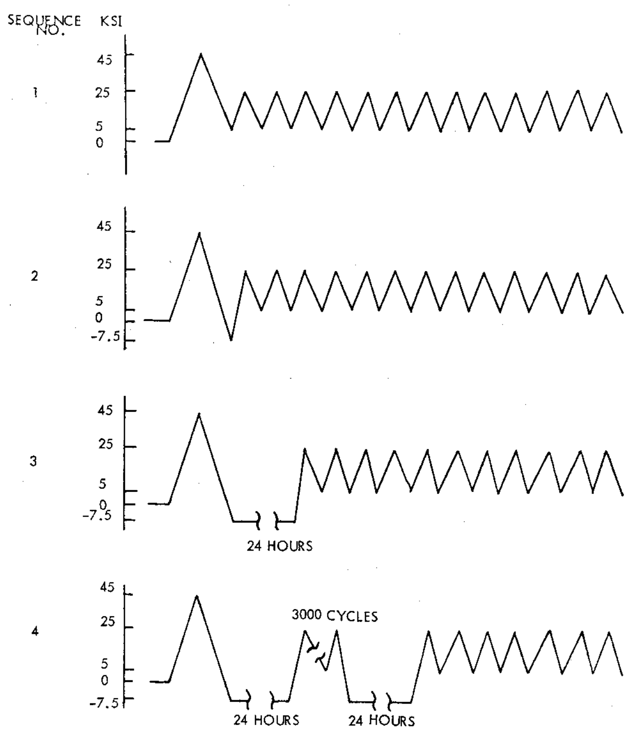

Fig. 2 Test sequences.